PROCEEDINGS OF THE ROYAL SOCIETY A

rspa.royalsocietypublishing.org

Research

Article submitted to journal

Subject Areas:
Biomechanics

Keywords:
Schwann Cell, Cell Mechanics, Traction Force Microscopy

Author for correspondence:
Christian Franck; Diane Hoffman-Kim
e-mail: franck@brown.edu; dhk@brown.edu

3D Traction Forces of Schwann Cells on Compliant Substrates

Cristina López-Fagundo,[1,†,‡] Eyal Bar-Kochba,[2,†] Liane L. Livi,[1] Diane Hoffman-Kim,[1,2,3,4], and Christian Franck[2,3]

[1]Department of Molecular Pharmacology, Physiology and Biotechnology, Providence, Rhode Island, USA, [2]School of Engineering, Brown University, Providence, Rhode Island, USA, and [3]Center of Biomedical Engineering, Brown University, Providence, Rhode Island, USA, and [4] Brown Institute for Brain Science, Providence, Rhode Island, USA

1. Supplementary Material

(a) Statistical analysis

Data were subjected to the Shapiro-Wilk normality test, to verify that the distribution of the data was normal, $p > 0.05$. For groups with normal distributions, parametric tests (one-way analysis of variance (ANOVA) for three or more groups or Students t-test for two groups) were used to compare the means. Post Hoc analyses (Tukey) for equal variance in the population were also employed for multiple comparison of the means and their interactions. For groups with non-normal distributions, non-parametric tests (Kruskal-Wallis one-way ANOVA on ranks for three or more groups or Welch's t-test for two groups) were used to compare the means. Post Hoc analyses (Dunn's) for unequal variance in the population were also employed for multiple comparison of the means and their interactions. A $p < 0.05$ was considered to be significant. The geometric mean, μ_g, and geometric mean absolute deviation, MAD, (error bars) that are reported in this study are defined as

$$\mu_g = \left(\prod_{i=1}^{n} x_i \right)^{1/n} \tag{1.1}$$

and

† Cristina López-Fagundo and Eyal Bar-Kochba contributed equally to this work.

‡ Current Address: Bone and Stem Cell Research Group, Competence Center for Applied Biotechnology and Molecular Medicine, University of Zürich, Winterthurerstr. 190 CH-8057, Zürich, Switzerland

Royal Society Publishing
Informing the science of the future

$$MAD = \left(\prod_{i=1}^{n} |x_i - \mu_g| \right)^{1/n} \tag{1.2}$$

All statistical tests, including power analysis were performed using SigmaPlot 12.3 (Systat Software Inc).

(b) Mechanical characterization of polyacrylamide gels

The elastic moduli of polyacrylamide (PA) gels were measured using an unconfined uniaxial compression test and a custom built compression testing apparatus. PA gels were cast using circular molds of 16 mm in diameter and 10 mm in height (McMaster Carr) and allowed to polymerize at room temperature for 30 – 40 minutes. The resulting cylindrical specimens were submerged in deionized water for 24 hours prior to testing to match the experimental cell time-lapse conditions. Samples were immersed in deionized water in a 35 mm culture dish (Corning Inc.) and covered with a 25 mm diameter, 1 mm thick polystyrene disc. This step was performed while the culture dish was located within the sample holder of the testing apparatus, consisting of a centrally positioned linear actuator (Series A, Ultramotion) equipped with a built-in encoder that provided displacement (strain) feedback. A tension/compression force transducer (LCFA-50G, Omega Engineering Inc.) attached to the moving end of the linear actuator provided force (stress) feedback during the compression of the sample. Prior to testing, the center of the PA gel sample was aligned along the central axis of the linear actuator and force transducer to ensure purely uniaxial stress conditions. Each sample was compressed at a strain rate of 0.02 s^{-1} while being monitored to ensure that the circumferential walls were free to expand. The engineering stress (σ) is calculated as the measured force divided by the circular contact area, and the engineering strain is calculated as the sample's change in height divided by its original height. Fig. S1 (inset) shows the loading stress-strain curve for a typical PA sample. The elastic modulus is calculated for each sample from the stress-strain curve using the relationship

$$E = \frac{\sigma}{\epsilon} = \frac{F/A}{\Delta h/h}. \tag{1.3}$$

The mechanical compression results are summarized in Fig. S1. The Poisson's ratio is taken to be 0.45, a value that falls within the typical range of values chosen for TFM studies [1, 2].

(c) Global force and moment balance

Net forces and moments acting on different control volumes within the PA gels satisfied static equilibrium. Under all conditions and time points the force and moments magnitudes were on the order of $10^{-9} - 10^{-6}$ N, and $10^{-14} - 10^{-11}$ N·m, which is consistent with our zero traction, zero displacement noise floor measurements. These numbers are similar to our previously reported values [3].

(d) Automated calculation of the Schwann cell surface boundary

The cellular surface boundary was determined from the flourescently labeled cell membrane. The sum intensity projection along the x_3 axis of the volume stack was computed. Following the application of a median filter to remove noise, contrast adjustment, and intensity normalization, the image was thresholded such that any values of less than than 90% of the maximum intensity were set to 0. A binary mask of the cell was generated by computing the largest connected component of the thresholded image. A course boundary of the binary mask was computed using the Moore-Neighbor tracing algorithm [4] and then smoothed using the algorithm developed by Taubin [5].

(e) Signal to noise measurements

The root mean squared traction values shown in eq. 6 in the main text are sensitive to the integration boundary used in the summation. To circumvent this issue, the integration boundary was chosen such that it maximized the signal to noise ratio (*SNR*) of the root mean squared tractions magnitude, $|\boldsymbol{T}|_{RMS}$. Fig. S2 shows a contour map of the tractions magnitude $|\boldsymbol{T}|$, the cell boundary (*white*), and all values interior and exterior of the integration boundary (*pink*), ∂B are defined as B_S and B_N. The signal-to-noise ratio, SNR, value is

$$SNR = \frac{signal}{noise} = \frac{(|\boldsymbol{T}|_{RMS})_{\subset B_S}}{(|\boldsymbol{T}|_{RMS})_{\subset B_N}}. \tag{1.4}$$

where $(|\boldsymbol{T}|_{RMS})_{\subset B_S}$ and $(|\boldsymbol{T}|_{RMS})_{\subset B_N}$ are the $|\boldsymbol{T}|_{RMS}$ values computed interior and exterior of ∂B respectively. To begin the optimization procedure, the initial *SNR* value, using ∂B of the cell boundary is computed. Each iteration thereafter, the ∂B is dilated and the SNR value is recomputed until convergence is reached. All traction values that are less than the noise level are not considered in the calculation for the $(\boldsymbol{T}_{RMS})_{\subset B_S}$. As an extra precautionary measure, any time point with a *SNR* value of less than two is excluded from the analysis. Additionally, the minimum resolvable traction is conservatively computed as a value that is less than $\mu_g + 2{\cdot}MAD$ of all of the samples binned by each elastic modulus. Table S1 summarizes the noise floor results for the tractions and displacements as computed by the above method.

2. Figures & Tables

Table S1. Noise floor results used to determine the signal-to-noise ratio or the image.

	Displacements (μm)		Tractions (Pa)	
E (Pa)	Shear ($\parallel$)	Normal ($\perp$)	Shear ($\parallel$)	Normal ($\perp$)
240	0.09	0.20	2.0	9.9
1700	0.06	0.14	15.9	81.1
4800	0.06	0.06	43.4	200

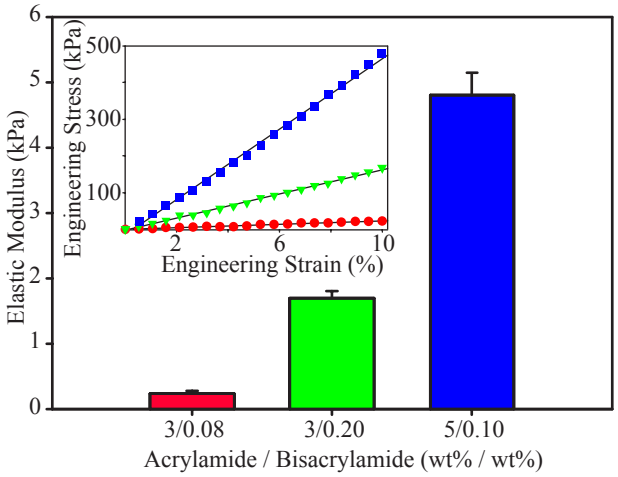

Figure S1. Polyacrylamide (PA) substrates were fabricated with three different physiologically relevant stiffnesses. Young's modulus for PA gels with different degree of crosslinking were calculated: (*red*) 0.24 $\pm$ 0.05 kPa , (*green*) 1.70 $\pm$ 0.09 kPa, and (*blue*) 4.80 $\pm$ 0.29 kPa. Stress-strain curve for polyacrylamide gels with different degrees of crosslinking was linear across stiffnesses (inset): (●) 3/0.08, (▼) 3/0.20, and (■) 5/0.10. (Online version in color.)

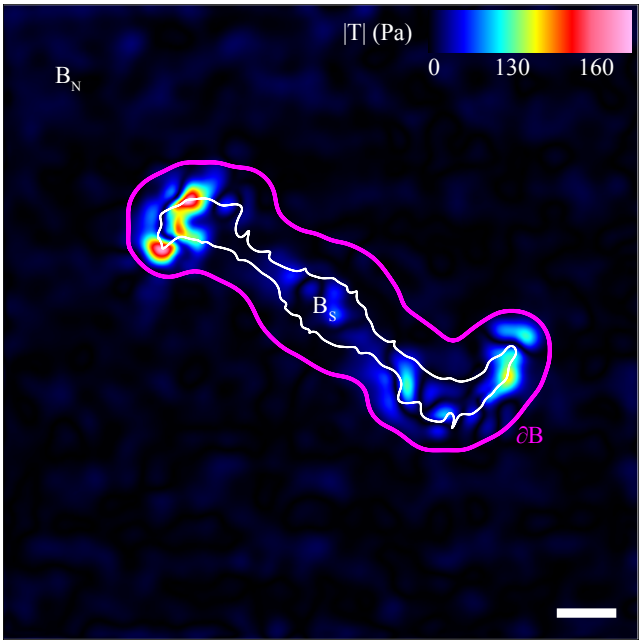

Figure S2. Surface contour map of a representative SC used to illustrate the integration boundary computation (*pink*, ∂B). The integration boundary was computed such that it maximized the signal to noise ratio of the root mean squared tractions magnitude. All values interior and exterior of the integration boundary are defined as B_N and B_S respectively. The cell surface boundary (*white*) was the initial guess for the optimization procedure. Scale bar represents 20 μm. (Online version in color.)

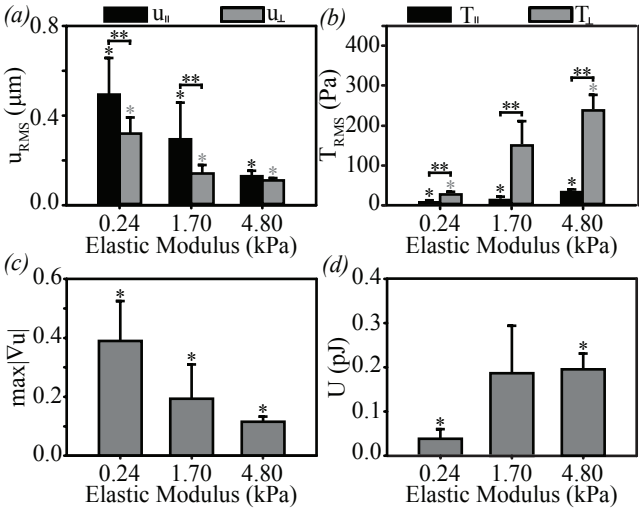

Figure S3. SC displacements, tractions, and strain energies varied with elastic moduli for the unpolarized morphology. Bar plots of the (*a*) root mean squared displacements magnitude (u_{RMS}), (*b*) root mean squared tractions (T_{RMS}), (*c*) maximum displacement gradient magnitude ($max|\nabla \boldsymbol{u}|$), and (*d*) strain energy (U) as a function of elastic modulus; 0.24 kPa (n $=$ 92), 1.70 kPa (n $=$ 65), and 4.80 kPa (n $=$ 22). The u_{RMS} and T_{RMS} values are split into their respective shear components ($u_{\parallel}, T_{\parallel}$) and normal components ($u_{\perp}, T_{\perp}$) (*black* and *grey* respectively). Geometric mean (μ_g) and geometric mean absolute deviation (*MAD*) are shown. $*$ indicates p $<$ 0.05 by one-way ANOVA on ranks across elastic moduli, and $**$ indicates p $<$ 0.001 by t-test between normal and shear components respectively.

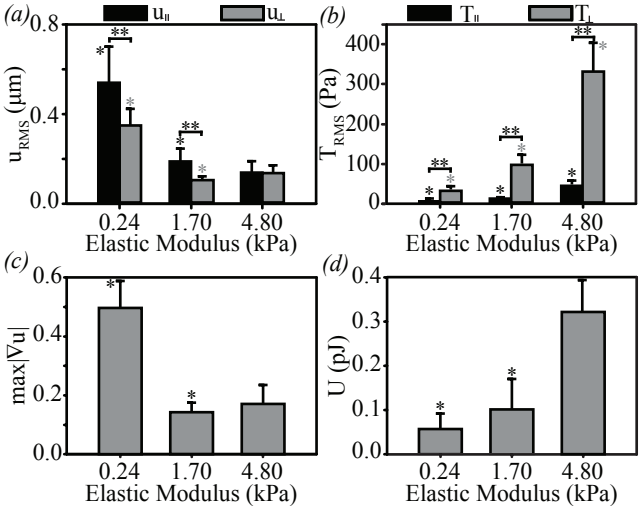

Figure S4. SC displacements, tractions, and strain energies varied with elastic moduli for the multipolar morphology. Bar plots of the (*a*) root mean squared displacements magnitude (u_{RMS}), (*b*) root mean squared tractions (T_{RMS}), (*c*) maximum displacement gradient magnitude ($max|\nabla \boldsymbol{u}|$), and (*d*) strain energy (U) as a function of elastic modulus; 0.24 kPa (n $=$ 63), 1.70 kPa (n $=$ 65), and 4.80 kPa (n $=$ 14). The $\boldsymbol{u}_{RMS}$ and T_{RMS} values are split into their respective shear components ($u_{\parallel}, T_{\parallel}$) and normal components ($u_{\perp}, T_{\perp}$) (*black* and *grey* respectively). Geometric mean (μ_g) and geometric mean absolute deviation (*MAD*) are shown. $*$ indicates p $<$ 0.05 by one-way ANOVA on ranks across elastic moduli, and $**$ indicates p $<$ 0.001 by t-test between normal and shear components respectively.

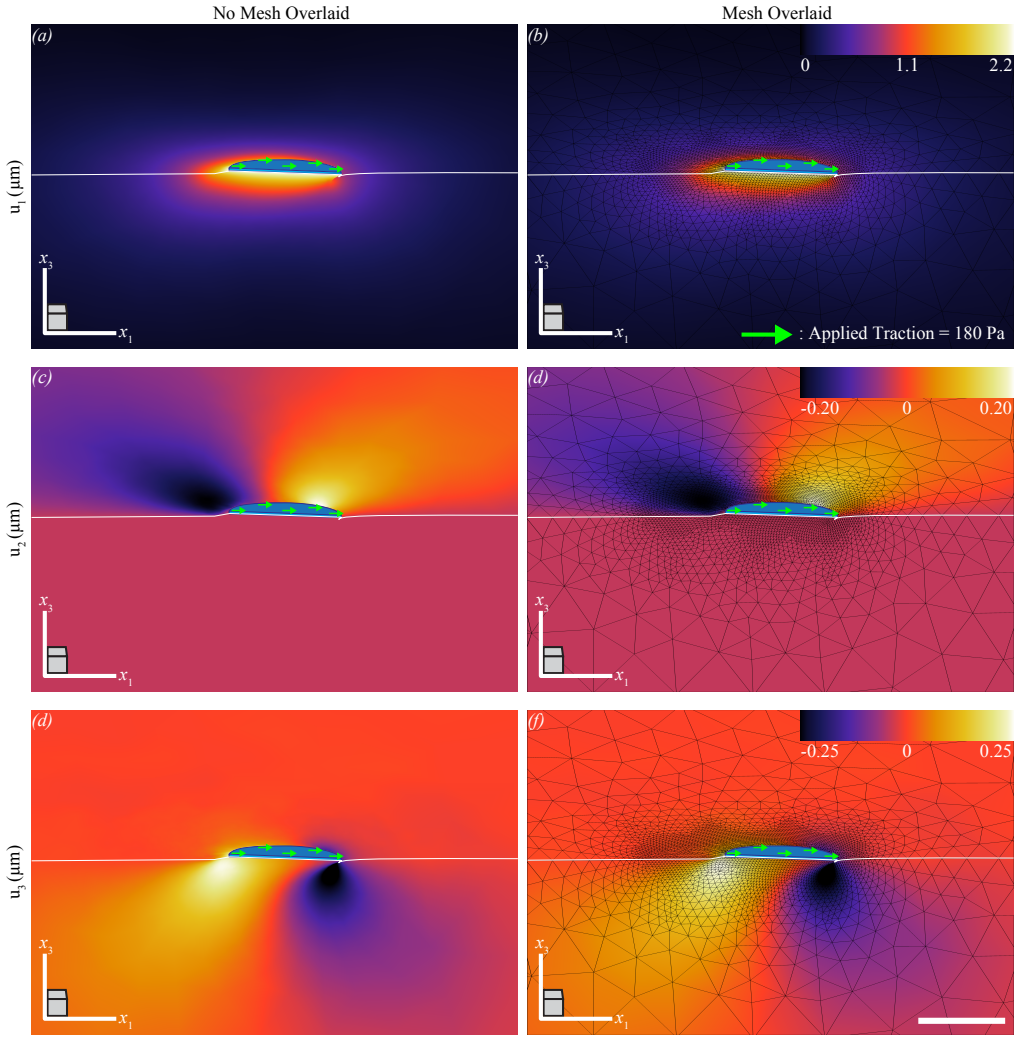

Figure S5. Finite element simulation results along the symmetry plane showing the displacement field induced in the deformed configuration of the E = 0.24 kPa PA gel. The displacement field is shown for the u_1 , u_2, and u_3 components with no mesh overlaid (*a*,*c*, and *e*) and with mesh overlaid (*b*, *d*, and *f*). The adhesion plaque was modeled as a rigid plate that is firmly bonded (surface-to-surface *TIE constraint) to the PA gel with a uniform shear traction (green) of magnitude 180 Pa applied to the top surface (using *DSLOAD) of the FA plaque (blue). The shear traction magnitude loading was determined by matching the maximum displacement magnitudes of the simulated to the experimentally observed ones. Surface Scale bar represents 5 μm. (Online version in color.)

Supporting References

1 del Álamo, J. C., Meili, R., Álvarez-González, B., Alonso-Latorre, B., Bastounis, E., Firtel, R. & Lasheras, J. C. 2013 Three-dimensional quantification of cellular traction forces and mechanosensing of thin substrata by fourier traction force microscopy. *PLoS ONE*, **8(9)**, e69 850. (doi:10.1371/journal.pone.0069850)

2 Engler, A. J., Griffin, M. A., Sen, S., Bönnemann, C. G., Sweeney, H. L. & Discher, D. E. 2004 Myotubes differentiate optimally on substrates with tissue-like stiffness pathological implications for soft or stiff microenvironments. *J. Cell Biol.*, **166**(6), 877–887. (doi:10.1083/jcb.200405004)

3 Maskarinec, S. A., Franck, C., Tirrell, D. A. & Ravichandran, G. 2009 Quantifying cellular traction forces in three dimensions. *Proc. Natl. Acad. Sci. USA*, **106**(52), 22 108–22 113. (doi:10.1073/pnas.0904565106)
4 Gonzalez, R. C., Woods, R. E. & Eddins, S. L. 2009 *Digital image processing using matlab*, vol. 2. Gatesmark Publishing Knoxville.
5 Taubin, G. 1995 A signal processing approach to fair surface design. In *Proceedings of the 22nd annual conference on computer graphics and interactive techniques*, pp. 351–358. ACM.